

Thermal softening induced subduction initiation at a passive margin

Daniel Kiss, Lorenzo Candioti, Thibault Duretz, Stefan M Schmalholz

▶ **To cite this version:**

Daniel Kiss, Lorenzo Candioti, Thibault Duretz, Stefan M Schmalholz. Thermal softening induced subduction initiation at a passive margin. Geophysical Journal International, 2020, 220 (3), pp.2068-2073. 10.1093/gji/ggz572 . insu-02462658

HAL Id: insu-02462658

https://insu.hal.science/insu-02462658

Submitted on 31 Jan 2020

HAL is a multi-disciplinary open access archive for the deposit and dissemination of scientific research documents, whether they are published or not. The documents may come from teaching and research institutions in France or abroad, or from public or private research centers.

L'archive ouverte pluridisciplinaire **HAL**, est destinée au dépôt et à la diffusion de documents scientifiques de niveau recherche, publiés ou non, émanant des établissements d'enseignement et de recherche français ou étrangers, des laboratoires publics ou privés.

submitted to *Geophys. J. Int.*

Thermal softening induced subduction initiation at a passive margin

Dániel Kiss[1], Lorenzo G. Candioti[1], Thibault Duretz[2,1] and Stefan M. Schmalholz[1]

[1] *Institute of Earth Sciences, University of Lausanne, 1015 Lausanne, Switzerland*

[2] *Univ. Rennes, CNRS, Géosciences Rennes - UMR 6118, F-35000 Rennes, France*

SUMMARY

We present two-dimensional numerical simulations of convergence at a hyper-extended passive margin with exhumed sub-continental mantle. We consider visco-elasto-plastic deformation, heat transfer and thermo-mechanical coupling by shear heating and associated thermal softening due to temperature dependent viscosity. The simulations show subduction initiation for convergence velocities of 2 $\mathrm{cm.yr^{-1}}$, initial Moho temperatures of 525 $^{\circ}\mathrm{C}$ and maximal deviatoric stresses of ca. 800 MPa, around the Moho, prior to localisation. Subduction initiates in the region with thinned continental crust and is controlled by a thermally-activated ductile shear zone in the mantle lithosphere. The shear zone temperature can be predicted with a recently published analytical expression. The criterion for subduction initiation is a temperature difference of at least 225 $^{\circ}\mathrm{C}$ between predicted temperature and initial Moho temperature. The modelled forced subduction broadly agrees with geological data and reconstructions of subduction during closure of the Piemont-Liguria basin, caused by convergence of the European and Adriatic plates during the Alpine orogeny.

Key words: Subduction initiation, thermal softening, shear heating, numerical modelling, thermo-mechanics.

1 INTRODUCTION

Subduction is an essential feature of plate tectonics, however, the processes controlling subduction initiation (SI) are still contentious (e.g. Vlaar & Wortel, 1976; Gurnis et al., 2004; Stern & Gerya, 2018). SI mechanisms are commonly classified as induced (i.e. caused by plate motions far away from the SI site) and spontaneous (i.e. caused by forces originating at the SI site; e.g. Stern, 2004). We focus here on induced SI at a passive margin with exhumed sub-continental mantle (e.g. Peron-Pinvidic & Manatschal, 2009). SI requires the formation of a major shear zone that transects the lithospheric mantle. Such shear zone could be pre-defined by inherited trans-lithospheric weak zones (e.g. Tommasi et al., 2009) or could be generated spontaneously by softening mechanisms (see recent review of Stern & Gerya, 2018), such as shear heating and associated thermal softening (e.g. Thielmann & Kaus, 2012), grain size reduction and microstructural damage (e.g. Bercovici & Ricard, 2012; Mulyukova & Bercovici, 2018) or softening due to increased water content along fluid pathways (e.g. Regenauer-Lieb et al., 2001). Out of the many softening mechanisms proposed to be important for SI, thermal softening is of particular interest because it (i) must occur due to energy conservation and temperature-dependent rock strength, and (ii) requires no additional assumptions about microscale processes such as grain size distribution and evolution or permeability structure and evolution. Recently, Kiss et al. (2019) presented a new analytical expression that predicts the quasi-constant temperature in a ductile shear zone that formed spontaneously by thermal softening. Their temperature prediction does not require any information of the shear zone itself, such as its thickness, stress or strain rate. Their prediction was validated with one-dimensional (1D), 2D and 3D numerical simulations, considering dislocation creep in a homogeneous material under constant ambient temperature. Kiss et al. (2019) speculated that their estimate is also applicable for visco-elasto-plastic deformation of the lithosphere, exhibiting heterogeneous material properties, due to crust and mantle, and considerable ambient temperature variation across the lithosphere. Furthermore, Kiss et al. (2019) argued that thermal softening may likely trigger SI at passive margins for convergence velocities on the order of a few centimeters per year. Here, we present 2D thermo-mechanical numerical simulations of convergence at a passive margin and show that (i) the expression of Kiss et al. (2019) indeed predicts the temperature in lithospheric mantle shear zones caused by thermal softening and (ii) induced SI by thermal softening indeed occurs for laboratory-derived flow laws, natural convergence velocities and realistic temperatures. We argue that our model is applicable to SI during closure of the Piemont-Liguria basin, caused by convergence of the European and Adriatic plates during the Alpine orogeny.

2 METHODS

2.1 Mathematical model

Our model is based on continuum mechanics (e.g. Mase & Mase, 1970; Turcotte & Schubert, 2014). We assume slow, incompressible deformation under gravity. We consider visco-elasto-plastic deformation assuming a Maxwell visco-elastic model and a Drucker-Prager brittle-plastic yield criterion. We consider heat transfer by conduction and advection, and heat production by shear heating and radiogenic decay. Heat transfer and deformation are coupled by shear heating, because dissipative work is converted into heat, required by the conservation of energy. Topography evolution is enabled by a free-surface, where erosion and sedimentation is mimicked by a linear diffusion of the topography. The applied equations and numerical method are described in the supplementary material.

Considering dislocation creep and velocity driven shearing, Kiss et al. (2019) show that the temperature in the shear zone, caused by thermal softening, always approaches a quasi-constant temperature that increases only slightly with deformation time, t. This temperature, T_{SH}, is predicted by:

$$T_{\mathrm{SH}} \approx -1.13\,\frac{Q}{nR}\left[\ln\left(\frac{\Delta v^2 nR}{\lambda Q}A^{-\frac{1}{n}}\left\{\frac{\Delta v}{\sqrt{\kappa t}}\right\}^{\frac{1}{n}-1}\right)+1.1\right]^{-1}. \tag{1}$$

where Δv is the far-field velocity difference (either for pure or simple shear); all other flow law and thermal parameters are given in Table S1.

2.2 Model configuration

The model mimics a hyper-extended passive margin with exhumed sub-continental mantle (Fig. 1a). The model is 1500 km wide and 400 km deep. In the exhumed mantle domain (left model side), the lithosphere is 90 km thick. The mantle flow law is for dry olivine with a combination of dislocation, diffusion and Peierls creep (Kameyama et al., 1999; Hirth & Kohlstedt, 2003) (Fig. 1a). The continental lithosphere has a 20 km thick upper crust with a flow law for Westerly granite (Carter & Tsenn, 1987). The lower crust is 10 km thick with a flow law for Maryland diabase (Mackwell et al., 1998). In the middle of the model the crust thins gradually to zero thickness towards the exhumed mantle domain within a 100 km wide zone (Fig. 1a). The lithosphere is initially in isostatic equilibrium generating an initial topographic difference between regions of exhumed mantle and unthinned crust of 5 km. The depth of the lithosphere-asthenosphere boundary below the unthinned crust is 123 km.

We apply free slip boundary conditions at the bottom and at the right model sides. The top boundary is a free surface. At the left boundary we apply a constant horizontal inflow velocity in the upper 200 km and a constant outflow velocity in the lower 200 km, so that the vertically-integrated velocity

is zero (e.g. Erdős et al., 2014). We apply a constant temperature of 15 $^{\circ}\mathrm{C}$ at the free surface, constant 1350 $^{\circ}\mathrm{C}$ at the model bottom and zero heat flux on the two sides. The asthenosphere is initially set to $T = 1350\ ^{\circ}\mathrm{C}$ and the initial temperature in the lithosphere is the equilibrium temperature. We apply different thermal conductivities in the crust to vary slightly the initial Moho (i.e. crust-mantle boundary) temperature (Table S1).

We performed four simulations: (1) with a 525 $^{\circ}\mathrm{C}$ initial Moho temperature and 2 $\mathrm{cm.yr}^{-1}$ convergence velocity, (2) 550 $^{\circ}\mathrm{C}$ initial Moho temperature and 2 $\mathrm{cm.yr}^{-1}$ convergence velocity, (3) 550 $^{\circ}\mathrm{C}$ initial Moho temperature and 4 $\mathrm{cm.yr}^{-1}$ convergence velocity, (4) without shear heating, 525 $^{\circ}\mathrm{C}$ initial Moho temperature, 2 $\mathrm{cm.yr}^{-1}$ convergence velocity (see also supplementary figures S1 to S4).

3 RESULTS

In simulation (1) visco-elastic stresses build up during the initial stages of convergence to reach the brittle-plastic yield and steady-state viscous flow stress (Fig. 1b and d). The evolving stress field shows the highest deviatoric stress magnitudes of ca. 800 MPa inside the lower crust around the brittle-ductile transition (i.e. transition from Drucker-Prager yield to any of the creep mechanisms) in the exhumed mantle region (Fig. 1b and d). The corresponding driving force per unit length (vertical integral of the difference between horizontal total stress, σ_{xx}, and lithostatic pressure) increases during stress build up to a maximal value of ca. $3.9 \times 10^{13}\ \mathrm{N.m}^{-1}$ (supplementary Fig. S5). Initially, convergence is characterized by distributed thickening and associated dissipative heating, resulting in a ca. 75 $^{\circ}\mathrm{C}$ temperature rise around the Moho during the first 7 Myr (see 500 and 600 $^{\circ}\mathrm{C}$ isotherm of Fig. 1a and c). The lower crust is slightly folding causing small lateral stress variations (Fig. 1d). Shear heating and thermal softening around the Moho is locally efficient enough to cause the spontaneous development of a ductile shear zone ca. 150 km away from the transition between crust and exhumed mantle (at x-position 300 km in Fig. 1c, d, e and f). The temperature rise around the shear zone just below the Moho is ca. 200 $^{\circ}\mathrm{C}$ (Fig. 1e). Due to thermal softening and localization, stresses decrease by several hundred MPa (Fig. 1d and f), and the corresponding horizontal driving force decreases significantly during localization to a value of ca. $1.5 \times 10^{13}\ \mathrm{N.m}^{-1}$ (supplementary Fig. S5). During progressive convergence, the shear zone remains localised and forms a subduction zone, which subducts the exhumed mantle and parts of the thinned crustal region below the continental lithosphere with normal crustal thickness (Fig. 1g and h). Upper crustal material and sediments, deposited in the trench region, are subducted and lubricate the subduction interface. Once crustal material is subducted to ca. 90 km depth the small stresses, due to elevated temperatures and lubrication, do not generate significant shear heating and dissipation anymore (Fig. 2a).

For simulation (2) the initially 25 $^{\circ}\mathrm{C}$ higher Moho temperature results in lower effective viscos-

ity around the Moho, hence the dissipation is smaller due to the lower stresses. Thermal softening still impacts the deformation of the lithosphere, but causes localised thickening of the crust because a localised shear zone could not develop (Fig. 2b). A similar behaviour, that is a lower ambient temperature promoting stronger strain localisation, has been observed in 2D numerical studies of strike-slip deformation (Takeuchi & Fialko, 2012, 2013). For simulation (3) the initial Moho temperature is identical to the one in simulation (2) but the convergence velocity is increased to 4 $\mathrm{cm.yr}^{-1}$. For the higher convergence velocities, thermal softening causes again a localised shear zone and subduction similar to simulation (1) (Fig. 2c). For simulations (2) and (3) the initially 25 $^{\mathrm{o}}\mathrm{C}$ higher Moho temperatures result in lower stresses and driving forces (Figs. S1 to S5). For simulation (4) without shear heating there is no SI, only lithospheric scale folding whereby one of the lower crustal buckles amplifies into a drip-like structure at the same position where subduction initiates in simulations (1) and (3).

To test the temperature prediction of equation (1) we calculate T_{SH} for the mantle lithosphere for the applied parameters and specific times. Simulations (1) and (3) generated a localised ductile shear zone and corresponding values of T_{SH} are 754 $^{\mathrm{o}}\mathrm{C}$ and 786 $^{\mathrm{o}}\mathrm{C}$, respectively (Fig. 2a and c). Different values of T_{SH} are due to different velocities and/or simulation times corresponding to the displayed results (Fig. 2). We plot the temperature change, with respect to the initial temperature, of material points together with the isotherms for the corresponding value of T_{SH}, and $T_{\mathrm{SH}} \pm 100\ ^{\mathrm{o}}\mathrm{C}$. The maximal temperature rise is ca. 300 $^{\mathrm{o}}\mathrm{C}$ for the simulations with shear heating (1-3), that is dominantly due to shear heating. For the temperature comparison, we chose a time step for which the dissipation in the mantle was highest. Maximal dissipation in simulations (1-3) is on the order of 100 $\mu\mathrm{Wm}^{-3}$ which is approximately two orders of magnitude larger than heat production due to radioactive decay (Table S1). The isotherms of T_{SH} follow closely the ductile shear zones indicated by the band of high temperature increase in the mantle lithosphere (Fig. 2a and c). For both simulations, the temperature of the shear zone is within $\pm 100\ ^{\mathrm{o}}\mathrm{C}$ compared to T_{SH}, while the total temperature rise of the shear zone material is $> 250\ ^{\mathrm{o}}\mathrm{C}$. Therefore, equation (1) can reasonably accurate predict ductile shear zone temperature in models of visco-elasto-plastic lithosphere deformation (see also animation in supplementary material).

4 DISCUSSION

The equation for T_{SH} was tested by Kiss et al. (2019) with 1D, 2D and 3D numerical simulations for dislocation creep, homogeneous material properties and constant, homogeneous ambient temperature. For these conditions, Kiss et al. (2019) proposed that T_{SH} should be at least 50 $^{\mathrm{o}}\mathrm{C}$ higher than the ambient temperature to cause shear zone formation. The conditions in the presented lithosphere models are far more complex due to the visco-elasto-plastic rheological model, the heterogeneous material

properties and the significant temperature gradients across the lithosphere. To initiate subduction, a significant shear zone, associated with decreased deviatoric stress (Fig. 1f and h), must form in the mantle lithosphere (Fig. 2). Hence, we use the dislocation creep flow law parameters (Hirth & Kohlstedt, 2003) for the mantle to calculate T_{SH} representative for the mantle lithosphere. To illustrate the slight time dependence of T_{SH}: a time interval of 2.6 Myr generates an increase of T_{SH} of only 5 $^{\mathrm{o}}\mathrm{C}$ (Fig. 2a and b). We propose to use the initial Moho temperature as representative ambient temperature, because spontaneous ductile shear zone formation by thermal softening occurs most likely around the Moho where deviatoric stress in the mantle lithosphere and/or lower crust are highest. For our model configuration, the predicted T_{SH} of ca. 750 $^{\mathrm{o}}\mathrm{C}$ is ca. 225 $^{\mathrm{o}}\mathrm{C}$ higher than the initial Moho temperature of 525 $^{\mathrm{o}}\mathrm{C}$ in simulation (1). For simulation (2) with an initial Moho temperature of 550 $^{\mathrm{o}}\mathrm{C}$ a localised shear zone did not form. Hence, for the presented configuration, a critical temperature difference, ΔT_{c}, between T_{SH} and the initial Moho temperature, of at least 225 $^{\mathrm{o}}\mathrm{C}$ is required to generate a localised ductile mantle shear zone. The higher values of ΔT_{c} for lithospheric shear zone formation, compared to values for homogeneous material, are likely due to the fact that during lithospheric deformation additional modes of localised deformation are possible, such as localised folding or thickening. For values of $\Delta T_{\mathrm{c}} <$ ca. 225 $^{\mathrm{o}}\mathrm{C}$ localised thickening dominates in our simulations (Fig. 2b). However, the localised thickening is also associated with dissipation and thermal softening so that thermal softening also strongly affects lithosphere deformation even if it does not result in localised shear zone formation. For mantle flow laws other than applied in our models (e.g. Gouriet et al., 2019), that might provide lower deviatoric stress in the mantle lithosphere, slightly higher convergence velocities and/or lower initial Moho temperatures can compensate the lower stresses so that thermal softening could be significant also for "weaker" mantle flow laws.

The calculated temperatures of the mantle shear zones are between ca. 750 to 900 $^{\mathrm{o}}\mathrm{C}$ at depths between ca. 40 and 100 km, and are in broad agreement with temperature estimates for natural mantle shear zones (e.g. Vauchez et al., 2012).

In our models with SI the maximal values of the driving force are between 3.6×10^{13} and 3.9×10^{13} $\mathrm{N.m}^{-1}$ (Fig. S5). These values are significantly larger than estimates for ridge push, ca. 3.9×10^{12} $\mathrm{N.m}^{-1}$, and lower than maximal estimates for slab pull, or trench pull, of ca. 4.9×10^{13} $\mathrm{N.m}^{-1}$ (e.g. Turcotte & Schubert, 2014). It makes sense that the driving force for SI must be considerably larger than estimates for ridge push, because otherwise subduction should have already been initated at many passive margins worldwide, which is not the case, for example at passive margins along the west coast of Africa or the east coast of South America. Furthermore, the driving force in our models likely overestimates the driving force required for natural SI because we do not consider any pre-existing weak zones or additional microscale processes such as grain size reduction. The required stress for

strain localization in models with thermal softening coupled with softening due to grain size reduction is considerably smaller than the required stress in models with thermal softening only (Thielmann et al., 2015). In our models with SI, the maximal deviatoric stress of ca. 800 MPa around the Moho is high, but such values are in agrement with experimentally derived flow laws for a compressed strong mantle lithosphere and lower crust (e.g. Burov et al., 2006; Jain et al., 2017). We speculate that sufficiently high driving forces required for SI could be reached locally for a transient period on Earth due to effects such as geometrical stress focusing (e.g. laterally variable passive margin geometry or plate-rotation with radially increasing velocities) or stress concentrations due to material heterogeneities (e.g. laterally variable mantle strength due to variation in water fugacity or grain size).

Our model mimics a hyper-extended magma-poor passive margin with exhumed sub-continental mantle. Such margin is observed at the Iberia-Newfoundland margins and geologically reconstructed for margins of the Jurassic Piemont-Liguria basin between the European and Adriatic plates (e.g. Peron-Pinvidic & Manatschal, 2009; Mohn et al., 2010). Several studies argue that forced, convergence induced, subduction initiation was the mechanism to initiate subduction in the Piemont-Liguria basin, related to the northward migration of Africa. (e.g. De Graciansky et al., 2010; McCarthy et al., 2018). Furthermore, subduction started in the continental region of the distal Adriatic margin, because earliest Alpine high-pressure units are the Sesia-Dent Blanche crustal units, which are attributed to the former Adriatic margin (e.g. Manzotti et al., 2014). Forced subduction, with SI in the continental crustal region of a passive margin and subsequent subduction of exhumed mantle was proposed for the Western Alps and is in agreement with our model results. We, hence, argue that thermal softening was likely an important mechanism for SI in the Piemont-Liguria basin.

5 CONCLUSIONS

We show with 2D thermo-mechanical numerical simulations that induced SI occurs due to thermal softening at passive margins with exhumed sub-continental mantle. SI occurs for convergence velocities of 2 cm.yr^{-1}, Moho temperatures between 525 and 600 ^{o}C and maximal deviatoric stresses around the Moho of ca. 800 MPa. Subduction initiates in the margin region of thinned continental crust. The modelled SI is similar to geological reconstructions for the closure of the Piemont-Liguria basin during Western Alpine orogeny.

The maximal temperature in the ductile mantle shear zone can be predicted with an analytical expression (eq. 1). If the predicted temperature is at least 225 ^{o}C higher than the initial Moho temperature, then subduction initiation triggered by thermal softening is most likely to occur. The analytical solution can, hence, in principle be used as criterion for forced subduction initiation by thermal softening.

ACKNOWLEDGEMENT

We are grateful for the constructive reviews of Prof. Yuri Fialko and Prof. Taras Gerya. This work is supported by SNF project 200020-149380 and the University of Lausanne.

References

Bercovici, D. & Ricard, Y., 2012. Mechanisms for the generation of plate tectonics by two-phase grain-damage and pinning, *Physics of the Earth and Planetary Interiors*, **202**, 27–55.

Burov, E., Watts, A., et al., 2006. The long-term strength of continental lithosphere:" jelly sandwich" or" crème brûlée"?, *GSA today*, **16**(1), 4.

Carter, N. L. & Tsenn, M. C., 1987. Flow properties of continental lithosphere, *Tectonophysics*, **136**(1-2), 27–63.

Crameri, F., 2018. Scientific colour-maps.

De Graciansky, P.-C., Roberts, D. G., & Tricart, P., 2010. *The Western Alps, from rift to passive margin to orogenic belt: an integrated geoscience overview*, vol. 14, Elsevier.

Erdős, Z., Huismans, R. S., van der Beek, P., & Thieulot, C., 2014. Extensional inheritance and surface processes as controlling factors of mountain belt structure, *Journal of Geophysical Research: Solid Earth*, **119**(12), 9042–9061.

Gouriet, K., Cordier, P., Garel, F., Thoraval, C., Demouchy, S., Tommasi, A., & Carrez, P., 2019. Dislocation dynamics modelling of the power-law breakdown in olivine single crystals: Toward a unified creep law for the upper mantle, *Earth and Planetary Science Letters*, **506**, 282–291.

Gurnis, M., Hall, C., & Lavier, L., 2004. Evolving force balance during incipient subduction, *Geochemistry, Geophysics, Geosystems*, **5**(7).

Hirth, G. & Kohlstedt, D., 2003. Rheology of the upper mantle and the mantle wedge: A view from the experimentalists, *Inside the subduction Factory*, pp. 83–105.

Jain, C., Korenaga, J., & Karato, S.-i., 2017. On the yield strength of oceanic lithosphere, *Geophysical Research Letters*, **44**(19), 9716–9722.

Kameyama, M., Yuen, D. A., & Karato, S.-I., 1999. Thermal-mechanical effects of low-temperature plasticity (the peierls mechanism) on the deformation of a viscoelastic shear zone, *Earth and Planetary Science Letters*, **168**(1-2), 159–172.

Kiss, D., Podladchikov, Y., Duretz, T., & Schmalholz, S. M., 2019. Spontaneous generation of ductile shear zones by thermal softening: Localization criterion, 1d to 3d modelling and application to the lithosphere, *Earth and Planetary Science Letters*, **519**, 284–296.

Mackwell, S., Zimmerman, M., & Kohlstedt, D., 1998. High-temperature deformation of dry diabase with application to tectonics on venus, *Journal of Geophysical Research: Solid Earth*, **103**(B1), 975–984.

Manzotti, P., Ballevre, M., Zucali, M., Robyr, M., & Engi, M., 2014. The tectonometamorphic evolution of the sesia–dent blanche nappes (internal western alps): review and synthesis, *Swiss Journal of Geosciences*, **107**(2-3), 309–336.

Mase, G. E. & Mase, G., 1970. *Continuum mechanics*, vol. 970, McGraw-Hill New York.

McCarthy, A., Chelle-Michou, C., Müntener, O., Arculus, R., & Blundy, J., 2018. Subduction initiation without magmatism: The case of the missing alpine magmatic arc, *Geology*, **46**(12), 1059–1062.

Mohn, G., Manatschal, G., Müntener, O., Beltrando, M., & Masini, E., 2010. Unravelling the interaction between tectonic and sedimentary processes during lithospheric thinning in the alpine tethys margins, *International Journal of Earth Sciences*, **99**(1), 75–101.

Mulyukova, E. & Bercovici, D., 2018. A theoretical model for the evolution of microstructure in lithospheric shear zones, *Geophysical Journal International*, **216**(2), 803–819.

Peron-Pinvidic, G. & Manatschal, G., 2009. The final rifting evolution at deep magma-poor passive margins from iberia-newfoundland: a new point of view, *International Journal of Earth Sciences*, **98**, 1581–1597.

Regenauer-Lieb, K., Yuen, D. A., & Branlund, J., 2001. The initiation of subduction: criticality by addition of water?, *Science*, **294**(5542), 578–580.

Stern, R. J., 2004. Subduction initiation: spontaneous and induced, *Earth and Planetary Science Letters*, **226**(3-4), 275–292.

Stern, R. J. & Gerya, T., 2018. Subduction initiation in nature and models: A review, *Tectonophysics*, **746**, 173–198.

Takeuchi, C. S. & Fialko, Y., 2012. Dynamic models of interseismic deformation and stress transfer from plate motion to continental transform faults, *Journal of Geophysical Research: Solid Earth*, **117**(B5).

Takeuchi, C. S. & Fialko, Y., 2013. On the effects of thermally weakened ductile shear zones on postseismic deformation, *Journal of Geophysical Research: Solid Earth*, **118**(12), 6295–6310.

Thielmann, M. & Kaus, B. J., 2012. Shear heating induced lithospheric-scale localization: Does it result in subduction?, *Earth and Planetary Science Letters*, **359**, 1–13.

Thielmann, M., Rozel, A., Kaus, B., & Ricard, Y., 2015. Intermediate-depth earthquake generation and shear zone formation caused by grain size reduction and shear heating, *Geology*, **43**(9), 791–794.

Tommasi, A., Knoll, M., Vauchez, A., Signorelli, J. W., Thoraval, C., & Logé, R., 2009. Structural reactivation in plate tectonics controlled by olivine crystal anisotropy, *Nature Geoscience*, **2**(6), 423.

Turcotte, D. & Schubert, G., 2014. *Geodynamics*, Cambridge university press.

Vauchez, A., Tommasi, A., & Mainprice, D., 2012. Faults (shear zones) in the earth's mantle, *Tectonophysics*, **558**, 1–27.

Vlaar, N. & Wortel, M., 1976. Lithospheric aging, instability and subduction, *Tectonophysics*, **32**(3-

4), 331–351.

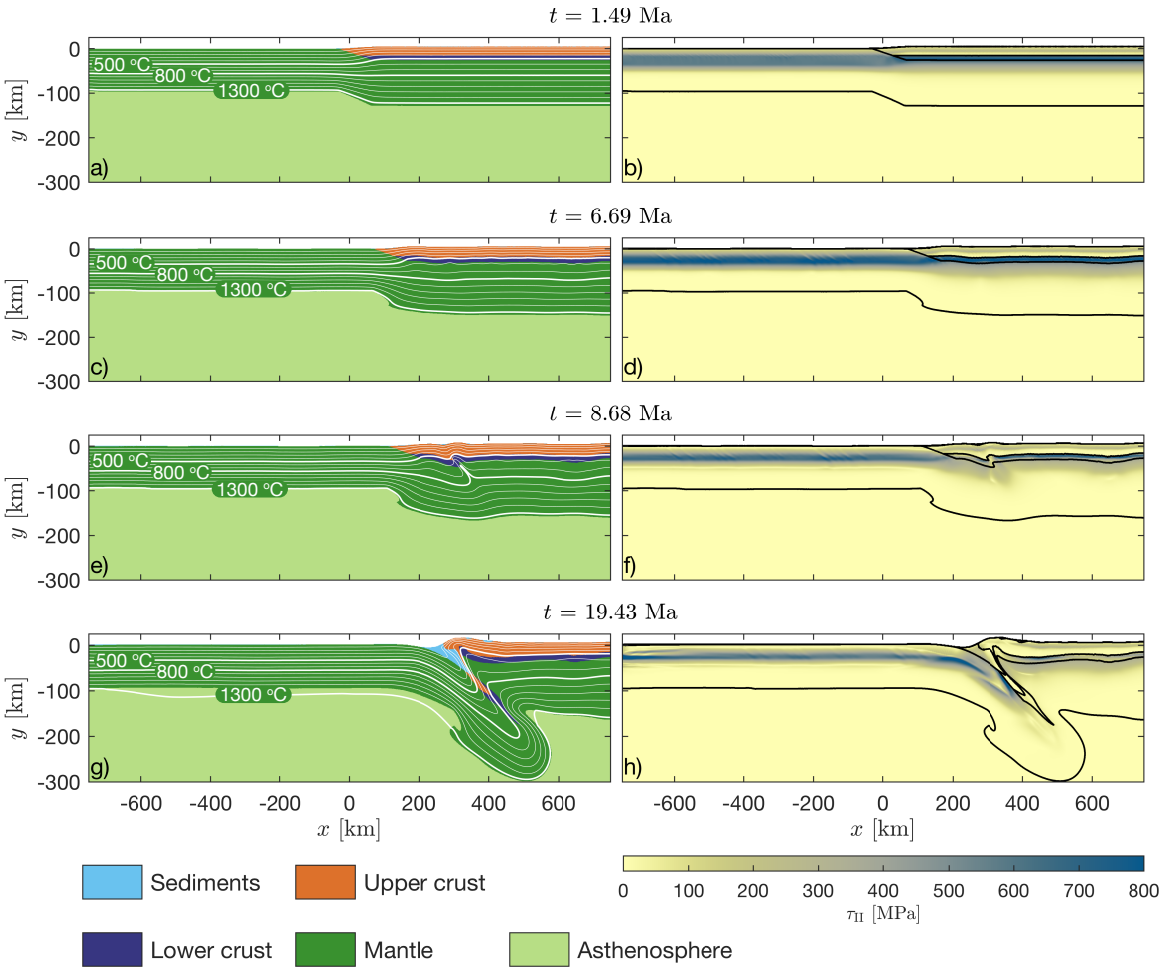


Figure 1. Evolution of model geometry (left column) and stress field (right column) for simulation (1). Left column: White lines indicate isotherms every 100 °C and colored fields indicate different model units; see legend below left column. Right column: Stress is quantified with second invariant of deviatoric stress tensor. Black lines indicate from bottom to top: lithosphere-asthenosphere boundary, Moho and upper-lower crust boundary. Colourmaps are from Crameri (2018).

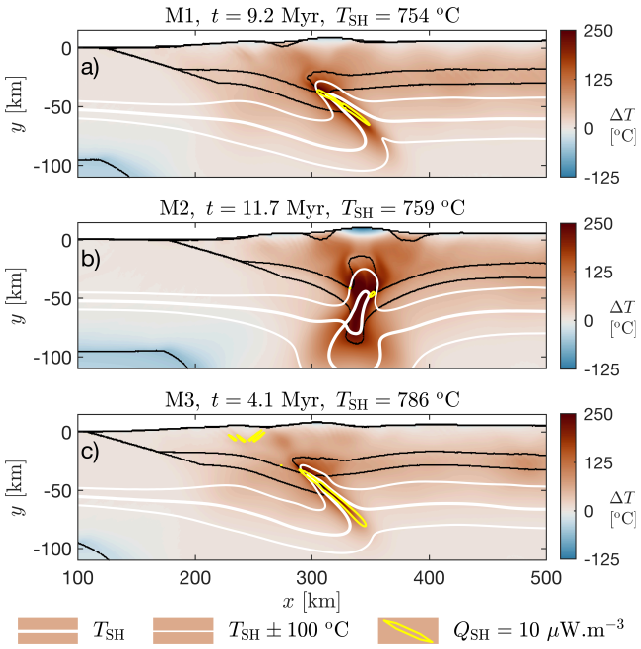


Figure 2. Colourplot of temperature change, with respect to initial temperature, of material points, ΔT, for models (1, a) to (3, c) at specific simulation times, t. For better visibility the colour bar is saturated at 250 °C, however, the maximal change is 312, 290 and 331 °C for models (1, a) to (3, c), respectively. Values of T_{SH} are calculated with equation (1) for parameters of mantle dislocation creep (Table S1), corresponding convergence velocity and simulation time. Isotherms are plotted for corresponding T_{SH} and $T_{\mathrm{SH}} \pm 100$ °C (see legend). The yellow contours bound the area with significant dissipation, $Q_{\mathrm{SH}} \geq 10$ μW.m^{-3}.